Optical measurement of cycle-dependent cell growth

Mustafa Mir[a,b,1], Zhuo Wang[a,b,1], Zhen Shen[c], Michael Bednarz[d], Rashid Bashir[a,e,f], Ido Golding[d,g], Supriya G. Prasanth[c], and Gabriel Popescu[a,d,f,2]

[a]Department of Electrical and Computer Engineering, [b]Quantitative Light Imaging Laboratory, Beckman Institute for Advanced Science and Technology, [c]Department of Cell and Developmental Biology, and [d]Department of Physics, Centre for the Physics of Living Cells, [e]Micro and Nanotechnology Laboratory, [f]Department of Bioengineering, University of Illinois, Urbana, IL 61801; and [g]Verna and Marrs McLean Department of Biochemistry and Molecular Biology, Baylor College of Medicine, Houston, TX 77030

Edited by Peter T. C. So, Massachusetts Institute of Technology, Cambridge, MA, and accepted by the Editorial Board June 24, 2011 (received for review January 10, 2011)

Determining the growth patterns of single cells offers answers to some of the most elusive questions in contemporary cell biology: how cell growth is regulated and how cell size distributions are maintained. For example, a linear growth in time implies that there is no regulation required to maintain homeostasis; an exponential pattern indicates the opposite. Recently, there has been great effort to measure single cells using microelectromechanical systems technology, and several important questions have been explored. However, a unified, easy-to-use methodology to measure the growth rate of individual adherent cells of various sizes has been lacking. Here we demonstrate that a newly developed optical interferometric technique, known as spatial light interference microscopy, can measure the cell dry mass of many individual adherent cells in various conditions, over spatial scales from micrometers to millimeters, temporal scales ranging from seconds to days, and cell types ranging from bacteria to mammalian cells. We found evidence of exponential growth in *Escherichia coli*, which agrees very well with other recent reports. Perhaps most importantly, combining spatial light interference microscopy with fluorescence imaging provides a unique method for studying cell cycle-dependent growth. Thus, by using a fluorescent reporter for the S phase, we measured single cell growth over each phase of the cell cycle in human osteosarcoma U2OS cells and found that the G2 phase exhibits the highest growth rate, which is mass-dependent and can be approximated by an exponential.

quantitative phase imaging | population growth | adherent cell mass | label free imaging

Single cell growth regulation has been described as "one of the last big unsolved problems in cell biology" (1), and the ability to measure the growth rate of single cells is integral to answering this question (2–5). The age-old debate is whether the growth rate is constant through the life cycle of a cell (linear growth) or grows proportionally with the cell mass (exponential growth) (6–12). Each growth pattern carries its own biological significance. If the growth is linear, cells do not need machinery to maintain homeostasis; conversely, exponential growth requires checkpoints and regulatory systems to maintain a constant size distribution (7). This need for regulation can be understood simply by considering two daughter cells of different sizes: Under exponential growth, the larger of the two would grow faster, and thus the variability would increase with each generation; therefore, a mechanism to regulate growth must be present. The reason that this debate has persisted despite decades of effort is primarily due to the lack of quantitative methods to measure cell mass with the required sensitivity. To distinguish an exponential pattern from a linear one, it has been calculated that a resolution of <6% in cell size is required (13).

Until recently, the state-of-the-art method to assess a single cell growth curve was by using Coulter counters to measure the volume of a large number of cells, in combination with careful mathematical analysis (13). For relatively simple cells such as *Escherichia coli*, traditional microscopy techniques have also been used to assess growth in great detail (14). In this type of method, the assumption is that volume is a good surrogate for mass; however, this assumption is not always valid, for example, due to variations in osmotic pressure (5). Recently, shifts in the resonant frequency of vibrating microchannels have been used to quantify the buoyant mass of cells flowing through the structures (2, 15). Using this approach, Godin et al. (2) have shown that several cell types grow exponentially; i.e., heavier cells grow faster than lighter ones. However, although this method is sensitive enough to measure bacteria growth, it cannot be applied to adherent cell lines. Later, Park et al. (3) extended this principle to allow mass measurements on adherent cells. This benefit comes at the expense of sensitivity—e.g., it cannot measure single bacterium growth—and throughput—i.e., it measures single cells at a time. An ideal method would perform parallel growth measurements on an ensemble of cells simultaneously and continuously over more than one cell cycle, quantify possible cell cycle phase-dependent growth, apply equally well to adherent and nonadherent cells, and work in a fully biocompatible environment (2, 13). Here we demonstrate that a unique imaging method developed in our laboratory, spatial light interference microscopy (SLIM; ref. 16), approaches these ideals.

The principle behind using interferometry to measure cell dry mass was established in the early 1950s, when it was recognized that the optical phase shift accumulated through a live cell is linearly proportional to the dry mass (nonaqueous content) of the cell and since then has been used by many groups to monitor cell dry mass (17–21). In the past decade or so, quantitative phase imaging methods have advanced rapidly (for example, refs. 22 and 23 and references therein), and new biological applications have been explored (24–26). However, despite these advances, two main limitations commonly affect the performance of quantitative phase imaging: (*i*) reduced contrast due to the speckle generated by the laser sources and (*ii*) the complexity of the experimental setups limits their adaptation in biological settings. SLIM overcomes these challenges by combining traditional, white light phase contrast microscopy with holography, thus providing speckle-free quantitative phase maps (for details on the operating principle of white light interferometry and SLIM, see refs. 16 and 27–29 and *Materials and Methods*).

Recently, it has been shown, both theoretically and experimentally, that the surface integral of the cell phase map is invariant to small osmotic changes (5), which establishes that quantitative

Author contributions: M.M., Z.W., R.B., S.G.P., and G.P. designed research; M.M., Z.W., Z.S., and M.B. performed research; Z.S., M.B., I.G., and S.G.P. contributed new reagents/analytic tools; M.M., Z.W., and G.P. analyzed data; and M.M., Z.W., and G.P. wrote the paper.

The authors declare no conflict of interest.

This article is a PNAS Direct Submission. P.T.C.S. is a guest editor invited by the Editorial Board.

Freely available online through the PNAS open access option.

[1]M.M. and Z.W. contributed equally to this work.

[2]To whom correspondence should be addressed. E-mail: gpopescu@illinois.edu.

This article contains supporting information online at www.pnas.org/lookup/suppl/doi:10.1073/pnas.1100506108/-/DCSupplemental.

phase imaging methods can be used for dry mass measurements. The dry mass density at each pixel is calculated as:

$$\rho(x,y) = \frac{\lambda}{2\pi\gamma}\phi(x,y),$$

where λ is the center wavelength, γ is the average refractive increment of protein (0.2 mL/g; ref. 5), and $\phi(x,y)$ is the measured phase. The total dry mass is then calculated by integrating over the region of interest (see *Materials and Methods* for details on this procedure). Remarkably, SLIM's path-length sensitivity, of 0.3 nm spatially (pixel to pixel) and 0.03 nm temporally (frame to frame; ref. 16), translates into spatial and temporal sensitivities of 1.5 and 0.15 fg/μm^2, respectively.

Results

To demonstrate that SLIM can recover cell growth results on a well-studied sample (2), we imaged *E. coli* cells growing on an agar substrate at 37 °C. The evolution of single cells was tracked by using the Schnitzcell semiautomatic software (Michael Elowitz, Caltech; see *Materials and Methods* for a detailed description).

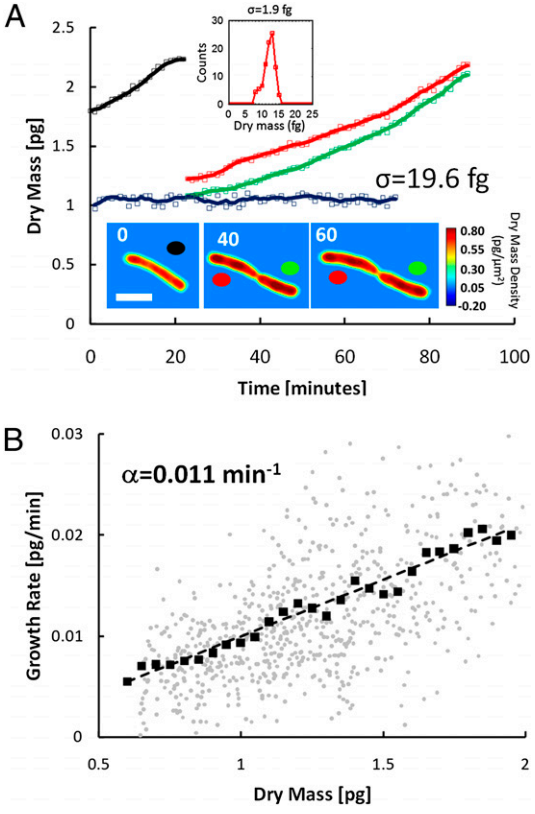

Fig. 1. SLIM measurements of *E. coli* growth. (*A*) Dry mass vs. time for a cell family. Growth curves for each cell are indicated by the colored circles on the images. Images show single cell dry mass density maps at the indicated time points (in minutes). (Scale bar: 2 μm.) (*Inset*) Histogram of the dry mass noise associated with the background of the same projected area as the average cell (SD σ = 1.9 fg is shown). The blue line is a fixed cell measurement, with SD of 19.6 fg. Markers indicate raw data, and solid lines indicate averaged data. (*B*) Growth rate vs. mass of 20 cells measured in the same manner. Faint circles indicate single data points from individual cell growth curves, dark squares show the average, and the dashed line is a linear fit through the averaged data; the slope of this line, 0.011 min^{-1}, is a measure of the average growth constant for this population. The linear relationship between the growth rate and mass indicates that, on average, *E. coli* cells exhibit exponential growth behavior.

Fig. 1*A* shows the dry mass growth curves for a family of *E. coli* cells. The negative mass densities are due to the fact that our measurements were always with respect to a baseline value of the surrounding medium, which is of zero average. As a control, we also measured fixed cells under the same conditions, from which we retrieved SD of 19.6 fg. Note that, because of the noise introduced by the culture environment, this error is larger than intrinsically allowed by the optical instrument. Fig. 1*B* shows the growth rate of 22 single cells as a function of mass, $dM(t)/dt$. The average of the data (black circles) shows that the growth rate is proportional to the mass, $dM(t)/dt = \alpha M(t)$, indicative of exponential growth. Before calculating the derivative, the raw data (markers) in Fig.1*A* was first time averaged (solid line) as detailed in the *Materials and Methods*. These results are in excellent agreement with recent measurements by Godin et al. (2) and demonstrate that SLIM can measure dry mass with the precision necessary for answering such biological questions. Note that our measurements were performed simultaneously on many individual cells and can be performed on adherent cells or bacterial biofilms, unlike the prior approaches, which can be either performed on suspended cells only (2) or on adherent cells but lacking the resolution to interrogate single bacteria (3). From our images, we can also retrieve the cell volume and, thus, extract information about the cell density. We found that the volume increase was also exponential with the same growth constant as for mass, 0.011 min^{-1} (Fig. S1). It can be seen that, on average, the volume is linearly proportional to mass, indicating constant average volumetric density. These results confirm the commonly accepted fact that, for this simple organism, in normal growth conditions, the volume and (because of the constant cell cross-section) cell length can be used as surrogates for mass (14).

Next we investigated the cell growth behavior in mammalian cells. To test the ability of SLIM to study growth in large populations of mammalian cells over more than a cell cycle, we imaged continuously for a 2-d period a 3.2 × 2.4-mm^2 field of view of a U2OS synchronized cell culture (Fig. 2). Note that for bigger cells, it is important to select the correct objective to ensure that the integral phase through the entire cell thickness is measured (for more details on this measurement, refer to *Materials and Methods* and *SI Materials and Methods*). Fig. 2 shows the results in terms of single-cell and ensemble growth curves. The results show that the mean cell mass evolves synchronously in time with the total mass of the entire population during the duration of a (mean) cell cycle, i.e., 22–26 h, after which it levels off. This finding indicates that after one cell cycle, the culture loses synchrony and the single cell mass is limited by mitosis. This measurement highlights the problems of using a synchronized population for cell cycle studies and reiterates the need for measuring single cells through an entire cell cycle in an asynchronous culture. To the best of our knowledge, this type of study, on such broad spatial and temporal scales, is not possible using any other existing method but is feasible by SLIM, as described below.

To study single cell growth in an asynchronous culture and obtain information about cell cycle-dependent growth, we used SLIM in combination with epifluorescence imaging. Note that because it interfaces with an existing microscope, SLIM shares the same optical path with all of the other channels of the microscope, including fluorescence. We imaged YFP–proliferating cell nuclear antigen (PCNA) human osteosarcoma (U2OS) cells stably expressing YFP–PCNA, which enabled us to monitor PCNA activity and thus progression through S phase via the fluorescence channel (Fig. S2). This activity was greatest during the DNA synthesis of the cell cycle and was observed in the localization of the fluorescence signal (its granular appearance), which revealed the S phase of the cell cycle (Fig. 3 *A* and *B*). This marker has been used extensively in the past to study cell cycle and replication dynamics (30–32). By using the fluorescence

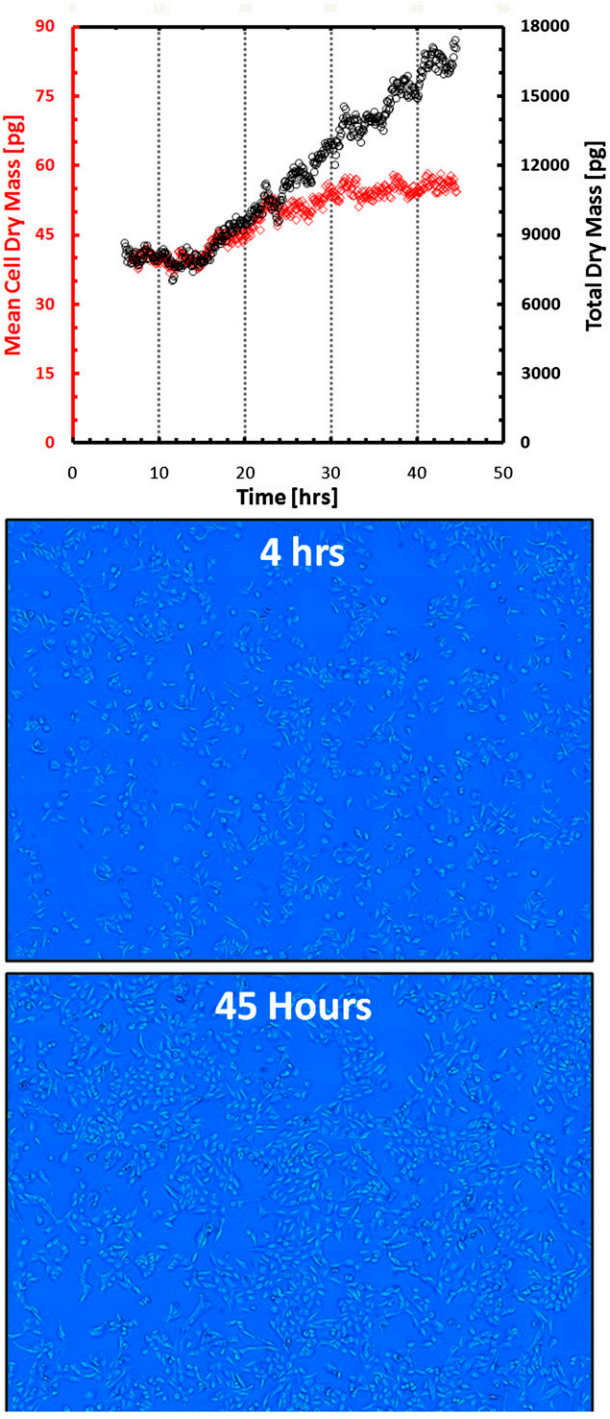

Fig. 2. SLIM measurement of synchronized U2OS cell culture over >2 d. Black shows dry mass vs. time for a synchronized cell population over a 3.2 × 2.4-mm^2 field of view obtained by montaging 8 × 8 microscope images. (10× objective, NA = 0.3). Red shows cell mean dry mass vs. time. Images show the field of view at 4 and 45 h; horizontal edge of image is 2.4 mm.

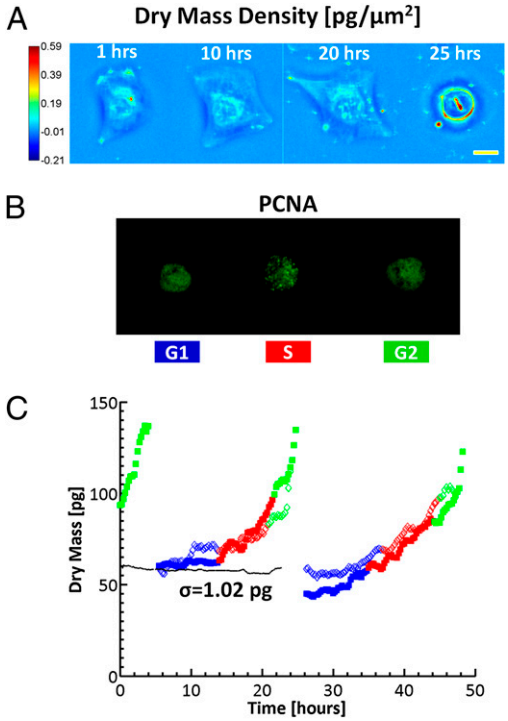

Fig. 3. SLIM measurement of U2OS growth over 2 d. (*A*) Dry mass density maps of a single U2OS cell over its entire cycle at the times indicated. (Scale bar: 25 μm.) Color bar indicates dry mass density in pg/μm^2. (*B*) Simultaneously acquired GFP fluorescence images indicating PCNA activity; the distinct GFP signal during S phase and the morphological changes during mitosis allow for determination of the cell cycle phase. (*C*) Dry mass vs. time for a cell family (i.e., 1→2→4 cells). The two different daughter cell lineages are differentiated by the filled and open markers; only one daughter cell from each parent is shown for clarity. Different colors indicate the cell cycle as reported by the GFP–PCNA fluorescence. The dotted black line shows measurements from a fixed cell, which has SD of 1.02 pg.

signal as one marker and the onset of mitosis as the second, it is possible to study cell growth in each phase of the cell cycle separately (Fig. S2). We measured a culture of U2OS cells for 51 h, scanning a 1.2 × 0.9-mm^2 area every 15 min and acquiring fluorescence data every 60 min, as described in detail in *Materials and Methods*. To avoid cell damage due to UV exposure, we minimized exposure time and power by using a highly sensitive EM-CCD as discussed in *Materials and Methods*. The consistent growth of the cells and the expected 24-h cell cycle (33) is a testament to the overall health of the culture. Fig. 3*C* shows typical growth curves measured from a single cell as it divides into two cells and then its daughters into four. This ability to differentiate between two daughter cells growing very close together, and to measure their dry mass independently, is a major advantage of SLIM over other methods, including microresonators, where such measurements are currently impossible to perform. As a control, we measured a fixed cell under the same conditions and found a SD of 1.02 pg, which is well within the acceptable error range. This error is larger than in the case of the *E. coli* measurements because the debris that exists in the mammalian cell culture contributes to the measurement noise. This debris is naturally occurring from cellular processes and can occasionally be observed passing through the field of view.

Our data show that U2OS cells are typically successful in doubling their mass by the end of G2 and that the daughter cells are typically half of the mass of their parents' doubled mass after mitosis. One unexpected observation is that the mass continued to increase during mitosis (Fig. S3). However, after this increase, upon completing cytokinesis, the two daughter cells decreased in mass and begin G1 at exactly half the mass of their parent at G2, which is the generally accepted behavior (13). See *SI Materials and Methods* and Fig. S3 for more details on mitosis.

Because of the cell cycle phase discrimination provided by YFP–PCNA, we can numerically synchronize our population a posteriori (Fig. 4*A*). To perform this numerical synchroniza-

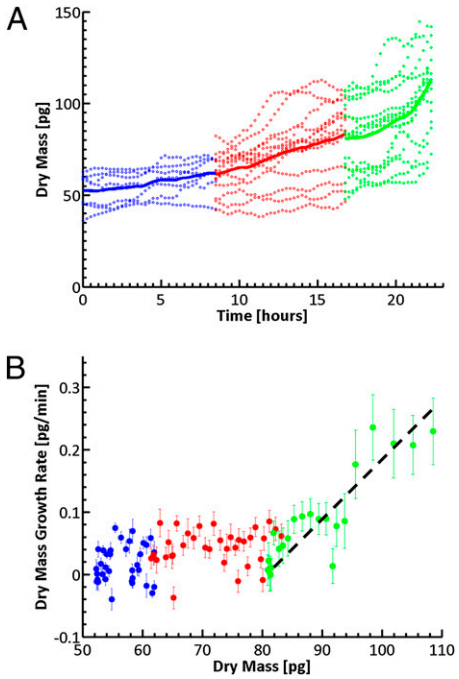

Fig. 4. (*A*) A posteriori synchronization combination of PCNA stain for S-phase determination and the visual determination of the onset of mitosis allow for the study of cell growth dependence on cell cycle phase in an asynchronous culture. Show is a G1-, S-, and G2-dependent mass growth as indicated by color. The cycles of the individual cells were aligned as described above; the *x* axis indicates the average time spent in the respective cell cycle phase by all. Open circles indicate single cell data, and solid lines indicate ensemble averages by cell cycle phase. It can clearly be seen that the cell growth is dependent on both the cell cycle phase and the current mass of the cell. (*B*) Dry mass growth rate vs. dry mass for the ensemble averages. It can be seen that G2 exhibits an exponential growth pattern compared with the relatively low growth measured in G1 and S phases.

tion, we found the average time of each cell cycle phase, and then all of the growth curves were resampled to fit the respective time windows. The dotted lines in Fig. 4*A* show the results for individual cells, and the solid lines indicate the ensemble-averaged data. Although this average was performed on a limited number of cells, clear differences in the growth behavior during the three cell cycle phases can be observed. Fig. 4*B* illustrates the differences in the growth rate between the G1, S, and G2 phases of the cell cycle. It can be seen that during G2, U2OS cells exhibit a mass-dependent growth rate that is approximately linear and thus indicates an exponential growth pattern. The large SD is to be expected from a small population set growing under heterogeneous conditions in terms of cell confluence. We anticipate that the interaction of a cell with its neighbors must play a role in cell growth. Even though further studies are required to make universal statements regarding mammalian cell growth, to our knowledge, cell cycle-dependent mass measurements have not been performed previously.

Discussion and Conclusions

Although population-level measurements on various cell types reveal exponential or linear growth patterns, we can expect large variability in results from different cell types. Our experiments on *E. coli* show that, on average, the cells follow an exponential pattern, although there is large variation among single cells in the same population. These types of variations are expected from a biological system and are of scientific interest in themselves; by studying the variations in the growth patterns of single cells under varying conditions, we may help elucidate some of the underlying regulatory processes. Because SLIM is an imaging technique, we may also simultaneously calculate the volume of regularly shaped cells such as *E. coli*. This ability allows us to explore questions of cell density and morphology and their roles in mass regulation. For *E. coli*, we found that the density is relatively constant, which is consistent with the exponential growth model for this organism (11). SLIM is also a powerful tool for studying the relationship of cell cycle stage, growth, and mass measurement in complex mammalian cells.

By taking advantage of the ability of SLIM to be implemented as an add-on to a commercial microscope, we can use all other available imaging channels. By combining SLIM with fluorescence, it is possible to combine the quantitative nature of interferometry with the specificity provided by fluorescent molecular probes. In conclusion, the results presented here establish that SLIM provides a number of advances with respect to existing methods for quantifying cell growth: (*i*) SLIM can perform parallel growth measurements on an ensemble of individual cells simultaneously; (*ii*) spatial and temporal correlations, such as cell–cell interactions, can be explored on large scales; (*iii*) in combination with fluorescence, specific chemical processes may be probed simultaneously; (*iv*) the environment is fully biocompatible and identical to widely used equipment; (*v*) the imaging nature of SLIM offers the ability to directly monitor cells and their surroundings, elucidating the nature of any artifacts and providing morphological information simultaneously; (*vi*) a lineage study is possible, i.e., a cell and its progeny may be followed; and (*vii*) measurements can be performed on cells ranging from bacteria to mammalian cells.

Materials and Methods

Cell Culture and Manipulation. *E. coli* MG1655 cells were cultured overnight in Luria broth. The overnight cultures were subcultured by dilution (100×) into commercial M9CA medium with thiamine (Teknova). After the culture reached an optical density (OD) of ∼0.1, the cells were concentrated to an OD of ∼0.4, and 2 μL of cell culture was pipetted onto a glass-bottom dish (In Vitro Scientific). The cells were covered by an agar slab (1.5% agarose, M9CA medium; 1-mm thickness), and 70 μL of H_2O was pipetted onto the edge of the dish (never in contact with the sample) to mitigate drying of the agar. The dish was then covered with a circular coverslip to reduce evaporation and transferred to the microscope for imaging. For the fixed cell measurements, 1 mL of ∼0.2-OD cell culture was centrifuged, and the resulting cell pellet was then mixed with 1 mL of 3.7% paraformaldehyde (Fisher Reagents). After 20 min the cells were washed twice with PBS (diluted from 10× stock; Teknova).

U2OS cells were grown in DMEM containing high glucose, supplemented with penicillin–streptomycin and 10% FBS (HyClone). Lipofectamine 2000 (Invitrogen)-mediated transfection was carried out in U2OS cells per the manufacturer's instructions, followed by G418 selection (600 μg/mL) to generate the YFP–PCNA stable cell line. For the synchronized population measurements, cells were arrested at the G1/S boundary by adding 2 mM thymidine. After 24 h, cells were washed three times with fresh medium, grown for 12 h, and incubated with 2 mM thymidine for an additional 24 h. Cells were then released for live cell imaging. For the fixed cell measurements, cells were fixed in 2% formaldehyde for 15 min at room temperature and then washed twice with PBS.

Cell Imaging. For the *E. coli* measurements, cells were kept at 37 °C with an incubator XL S1 W/CO_2 kit (Zeiss). Time-lapse SLIM images were acquired once a minute with a Zeiss Plan-Apochromat 63×/1.4 Oil PH3 M27. The sample was also scanned in *z* with a slice spacing of 0.280 μm and a total of 10 slices. The exposure time was 35 ms for each image at full lamp power (3,200 K, or 10.7 V), and the transmission shutter was closed before and after each scan.

For the synchronized U2OS measurements, cells were transferred to a "closed" cultivation chamber (POC-R cell cultivation system; Zeiss) and kept at 37 °C with an incubator XL S1 W/CO_2 kit (Zeiss) and a heating insert P S1/Scan stage (Zeiss) in L-15 medium (minus phenol red) containing 30% FBS. The medium was automatically refreshed every 4 h by using a syringe pump (Harvardpump 11 plus advanced dual syringe with dual RS-232; Harvard Apparatus) controlled by a Labview program developed in house. The pumping rate was set to 150 μL/min, and a total of 600 μL was pumped,

which is larger than the volume of the perfusion chamber, to ensure complete replacement of the growth medium. The imaging details are the same as the cell cycle study described below.

For the cell cycle study, cells were transferred to MatTek dishes (35-mm dishes; no. 1.5 glass thickness and 10-mm well diameter) and kept at 37 °C with an incubator XL S1 W/CO_2 kit (Zeiss) and a heating insert P S1/Scan stage (Zeiss) in L-15 medium (minus phenol red) containing 30% FBS. The dish was filled with culture medium (7 mL) and covered with a cover glass (diameter, 42 mm) to prevent possible evaporation. No noticeable medium loss was observed during the imaging interval of 2 d, because of the cover glass on top of the dish and the continuous supply of moisturized CO_2 gas into the chamber. Time-lapse SLIM images were acquired with a Zeiss EC Plan-Neofluar 10×/0.3 PH1 M27 objective, and the corresponding fluorescence images were recorded by using a Zeiss EC Plan-Neofluar 40×/0.75 PH2 objective. It is important to note that for the SLIM measurements, a lower numerical aperture was used here to ensure that the entire dry mass of the cell was captured, as explained in detail in *SI Materials and Methods* and Figs. S4 and S5. Excitation light for the fluorescence measurements was provided by an X-Cite 120XL package (120W HBO/Halide fluorescence illumination; Zeiss) and FITC filter set (Zeiss). Every 15 min, the sample was scanned in an 3 × 3 tile pattern to achieve a total field of view of 1.2 × 0.9 mm^2, while a *z* stack of seven slices was taken with slice spacing of 4 μm, which was optimal selected by Zeiss Axiovision software. The exposure time was 8 ms for each image at full lamp power (3,200 K, or 10.7 V), and the total scanning time for the multidimensional acquisition was 57 s. The transmission shutter was closed before and after each scan. At least 52 h of data were acquired in this manner for each experiment. The maximal projection was used for the processed *z* stack phase images to minimize the phase oscillatory behavior due to the defocusing effect, which is due to either the focus drift of the system or the movement of the cell. The fluorescence images were taken every hour in a 6 × 5 tile pattern to get a total field of view of 1.2 × 1.0 mm^2, centered on 3 × 3 tile pattern. A highly sensitive EM-CCD camera (PhotonMAX 512B; Princeton Instruments) located at the bottom port of the microscope was used for fluorescence image acquisition. The exposure time for each fluorescence image was 60 ms; the lamp power was set at 12.5% of the maximum lowest available for X-Cite 120XL (120W HBO/Halide fluorescence illumination; Zeiss), and the total scanning time was 21 s. The reflection shutter was controlled by Zeiss Axiovision software so that individual cells were exposed to the excitation light for only 60 ms at a time. A carefully adjusted reflection illumination field aperture assured that only minimum light leakage existed on the neighboring cells during mosaic scanning.

Image Segmentation. For the *E. coli* measurements, image segmentation was performed by using Schnitzcell software (kindly provided by M. Elowitz, Caltech). The software returns 2D parameters such as length and width of single cells, which can then be used to estimate volume. The cell is assumed to be a cylinder with spherical caps, and thus the volume can be calculated as $V = 4/3\pi r^3 + \pi r^2 * (l - 2r)$, where *r* is the radius and *l* is the length. The results of the segmentation could then be applied to our SLIM images to obtain the mass as described below.

For automatic segmentation of U2OS cells (Fig. 2), binary masks were prepared by using threshold, erosion, and dilation operations followed by a watershed algorithm; the software was implemented in MATLAB (MathWorks). The results from the automatic segmentation were used to measure mean parameters and cell number. However, because of the U2OS cells' complicated morphology, motility, and tendency to aggregate, accurate automatic tracking of single cells proved difficult. Although this problem may be overcome by more robust segmentation software, we resorted to manual segmentation to prove the utility of this method in a timely manner. Manual segmentation was performed by using the ROI manager available in ImageJ. Before calculating the mass, negative phase values were set to zero (as shown in Fig. S6) to minimize effects from the halo artifact.

Dry Mass Calculation and Analysis. The dry mass density at each pixel was calculated as

$$\rho(x,y) = \frac{\lambda}{2\pi\gamma}\phi(x,y),$$

where λ is the center wavelength; γ= 0.2 mL/g is the refractive increment of protein, which corresponds to an average of reported values (20); and $\phi(x,y)$ is the measured phase. The total dry mass was then calculated by integrating over the region of interest in the dry mass density map. Note that, even though in reality the refractive increment may vary slightly from cell type to cell type, this variation will only change the absolute value of the mass; i.e., it will not change the shape of the growth curves, which are of the greatest interest here. To get a more accurate measurement of the true dry mass, the projected maximum of three *z* slices centered around the middle of each cell was used to calculated the dry mass density map. To automatically detect the center position in each *z* stack, the mean phase of each *z* slice was calculated, and the slice with the maximum mean value was chosen as the center slice (34). For the *E. coli* cells, a 5-min running average was applied to the growth data. The mass growth rate data from 20 first- and second-generation *E. coli* cells was then compiled and averaged as shown in Fig. 1. For the averaging, a bin width of 0.05 pg and 0.1 fl was used for the dry mass and volume, respectively. For the U2OS cells, a running average of the raw data was calculated, with a window size of 75 min. It can be seen in the fixed cell measurements for both systems that the SLIM system is stable enough to perform sensitive growth experiments.

Cell Cycle-Dependent Measurements. We accomplished cell cycle-dependent growth measurements by using multimodal imaging, i.e., combining simultaneous fluorescence and SLIM imaging. Thus, we showed that it is possible to study single cell growth during each phase of the cell cycle separately, in an asynchronous culture. We imaged YFP–PCNA transfected human osteosarcoma (U2OS) cells, which enabled us to monitor PCNA activity via the fluorescence channel. This activity is greatest during the DNA synthesis of the cell cycle and was observed in the localization of the fluorescence signal, which, thus, revealed the S phase of the cell cycle (Fig. S2). This information, along with the initiation and completion of mitosis, gives a clear indication of the cell cycle progression. Fig 3*C* illustrates how this procedure allows the assessment of cell growth during the different phases of a complete cell cycle; thus, in an unsynchronized population, by using the PCNA marker, we can group the cells according to their cycle phase, essentially achieving a posteriori synchronization (Fig. 4*A*), which, to our knowledge, can only be done with a combination of SLIM and fluorescence measurement. For the ensemble averages shown in Fig. 4*A*, the growth curve for each cell was interpolated to fit the average time spent in that part of the cell cycle by all of the cells included in the ensemble. It must be emphasized that a major advantage of using an optical microscopy method to measure cell growth is the ability to visually determine the nature of the mass changes. For example, because we could simultaneously measure the cell shape and projected area as well as detect the inclusion of debris in region of the cell, we could numerically correct for this inclusion.

Design Details of SLIM Module. Objectives used for this study were Zeiss EC Plan-Neofluar 10×/0.3 PH1 M27, Zeiss EC Plan-Neofluar 40×/0.75 PH2, and Zeiss Plan-Apochromat 63×/1.4 Oil PH3 M27. The intermediate image right after the objective and tube lens was directed to left port for SLIM, phase contrast, and epifluorescence imaging.

To match the illumination ring and the size of the liquid crystal phase modulator (LCPM), the intermediate image was relayed by a 4f system with a focal-length 150-mm doublet (Thorlabs) and a focal-length 200-mm doublet (Thorlabs). Fourier lens L1 (doublet with focal length of 300 mm; Thorlabs) and Fourier lens L2 (doublet with focal length of 500 mm; Thorlabs) formed another 4f system. The LCPM (array size 7.68 × 7.68 mm; Boulder Nonlinear; XY Phase series) was placed at the back focal plane of L1 and thus overlaid with the back focal plan of the objective and the illumination ring. A polarizer (Edmund Optics) was placed in front of the LCPM to make sure it worked in phase modulation mode. The camera was Zeiss AxioCam MRm (1,388 × 1,040 pixels; pixel size 6.45 × 6.45 μm).

Overall, SLIM has an additional 2.22× magnification outside the microscope. For a 40× objective, the overall magnification will be 88.89×, which results in 13.78 pixels per μm in the image plane. Thus, our CCD was oversampling the diffraction spot by a safe margin. The microscope was equipped with live cell environmental controls optimized for 4-plus-hour time studies, including the incubator XL S1 W/CO_2 kit (Zeiss), heating insert P S1/Scan stage (Zeiss), and POC-R cell cultivation system. The whole microscope was controlled by Axiovision (Zeiss) with multichannel, time-lapse, mosaic, and *z*-stack acquisition. The LCPM was controlled by the Labview-based software development kits (Boulder Nonlinear). A data acquisition system based on Labview (National Instruments) and NI-DAQ (National Instruments) was also developed in-house to synchronize the LCPM, and Axiovision. Matlab, and ImageJ were used for phase image processing and visualization.

ACKNOWLEDGMENTS. Schnitzcell software was kindly provided by M. Elowitz (Caltech), and silica beads were provided by A. Mihi and P. Braun. This work was supported by National Science Foundation (NSF) Grants CBET-0939511 (to G.P. and R.B.), CAREER 08-46660 (to G.P.), and 0843604

(to S.G.P.) and the Grainger Foundation (G.P.). Work in the I.G. laboratory is supported by National Institutes of Health Grant R01GM082837, Human Frontier Science Program Grant RGY 70/2008, and NSF Grant 082265 (Physics Frontiers Center: Center for the Physics of Living Cells).

1. Weitzman JB (2003) Growing without a size checkpoint. *J Biol* 2:3.
2. Godin M, et al. (2010) Using buoyant mass to measure the growth of single cells. *Nat Methods* 7:387–390.
3. Park K, et al. (2010) Measurement of adherent cell mass and growth. *Proc Natl Acad Sci USA* 107:20691–20696.
4. Mitchison JM (2005) Single cell studies of the cell cycle and some models. *Theor Biol Med Model* 2:4.
5. Popescu G, et al. (2008) Optical imaging of cell mass and growth dynamics. *Am J Physiol Cell Physiol* 295:C538–C544.
6. Cooper S (2006) Distinguishing between linear and exponential cell growth during the division cycle: single-cell studies, cell-culture studies, and the object of cell-cycle research. *Theor Biol Med Model* 3:10.
7. Mitchison JM (2003) Growth during the cell cycle. *Int Rev Cytol* 226:165–258.
8. Killander D, Zetterberg A (1965) Quantitative cytochemical studies on interphase growth. I. Determination of DNA, RNA and mass content of age determined mouse fibroblasts in vitro and of intercellular variation in generation time. *Exp Cell Res* 38: 272–284.
9. Killander D, Zetterberg A (1965) A quantitative cytochemical investigation of the relationship between cell mass and initiation of DNA synthesis in mouse fibroblasts in vitro. *Exp Cell Res* 40:12–20.
10. Mitchison JM, Novak B, Sveiczer A (1997) Size control in the cell cycle. *Cell Biol Int* 21: 461–463.
11. Cooper S (1991) *Bacterial Growth and Division* (Academic Press Ltd., London, United Kingdom).
12. Wells WA (2002) Does size matter? *J Cell Biol* 158:1156–1159.
13. Tzur A, Kafri R, LeBleu VS, Lahav G, Kirschner MW (2009) Cell growth and size homeostasis in proliferating animal cells. *Science* 325:167–171.
14. Reshes G, Vanounou S, Fishov I, Feingold M (2008) Cell shape dynamics in Escherichia coli. *Biophys J* 94:251–264.
15. Bryan AK, Goranov A, Amon A, Manalis SR (2010) Measurement of mass, density, and volume during the cell cycle of yeast. *Proc Natl Acad Sci USA* 107:999–1004.
16. Wang Z, et al. (2011) Spatial light interference microscopy (SLIM). *Opt Express* 19: 1016–1026.
17. Rappaz B, et al. (2009) Noninvasive characterization of the fission yeast cell cycle by monitoring dry mass with digital holographic microscopy. *J Biomed Opt* 14:034049.
18. Sokol RJ, Wales J, Hudson, G, 2nd, Goldstein D, James NT (1991) Cellular dry mass during macrophage development in malignant lymphoma. *Anal Quant Cytol Histol* 13:379–382.
19. Davies HG, Wilkins MH (1952) Interference microscopy and mass determination. *Nature* 169:541.
20. Barer R (1952) Interference microscopy and mass determination. *Nature* 169:366–367.
21. Brown AF, Dunn GA (1989) Microinterferometry of the movement of dry matter in fibroblasts. *J Cell Sci* 92:379–389.
22. Depeursinge C (2006) *Digital Holography Applied to Microscopy Digital Holography and Three-Dimensional Display*, ed Poon T-C (Springer, New York), p 98.
23. Ding H, Popescu G (2011) Coherent light imaging and scattering for biological investigations. *Coherent Light Microscopy*, Springer Series in Surface Sciences, eds Ferraro P, Wax A, Zalevsky Z (Springer, Berlin), pp 229–265.
24. Park YK, et al. (2010) Metabolic remodeling of the human red blood cell membrane. *Proc Natl Acad Sci USA* 107:1289–1294.
25. Park YK, et al. (2010) Measurement of red blood cell mechanics during morphological changes. *Proc Natl Acad Sci USA* 107:6731–6736.
26. Ding HF, Wang Z, Nguyen F, Boppart SA, Popescu G (2008) Fourier transform light scattering of inhomogeneous and dynamic structures. *Phys Rev Lett* 101:238102.
27. Wang Z, Popescu G (2010) Quantitative phase imaging with broadband fields. *Appl Phys Lett* 96:051117.
28. Wang Z, et al. (2010) Topography and refractometry of nanostructures using spatial light interference microscopy. *Opt Lett* 35:208–210.
29. Ding HF, Popescu G (2010) Instantaneous spatial light interference microscopy. (Translated from English). *Opt Express* 18:1569–1575.
30. Leonhardt H, et al. (2000) Dynamics of DNA replication factories in living cells. *J Cell Biol* 149:271–280.
31. Essers J, et al. (2005) Nuclear dynamics of PCNA in DNA replication and repair. *Mol Cell Biol* 25:9350–9359.
32. Somanathan S, Suchyna TM, Siegel AJ, Berezney R (2001) Targeting of PCNA to sites of DNA replication in the mammalian cell nucleus. *J Cell Biochem* 81:56–67.
33. Thomas N, et al. (2004) Characterization and gene expression profiling of a stable cell line expressing a cell cycle GFP sensor. *Cell Cycle* 4:191–195.
34. Dubois F, Schockaert C, Callens N, Yourassowsky C (2006) Focus plane detection criteria in digital holography microscopy by amplitude analysis. *Opt Exp* 14:5895–5908.